Available online at www.sciencedirect.com
ScienceDirect
Nuclear Instruments and Methods in Physics Research A 579 (2007) 614–622
NUCLEAR INSTRUMENTS & METHODS IN PHYSICS RESEARCH Section A
www.elsevier.com/locate/nima

p-Bulk silicon microstrip sensors and irradiation

Y. Unno[a,*], S. Terada[a], T. Kohriki[a], Y. Ikegami[a], K. Hara[b], K. Inoue[b], A. Mochizuki[b], K. Yamamura[c], K. Sato[c]

[a]*Institute of Particle and Nuclear Study, KEK, Oho 1-1, Tsukuba, Ibaraki 305-0801, Japan*
[b]*Institute of Physics, University of Tsukuba, Tsukuba 305-8571, Japan*
[c]*Solid State Division, Hamamatsu Photonics K.K., 1126-1, Ichino-cho, Hamamatsu City 435-8558, Japan*

Available online 24 May 2007

Abstract

Anticipating the requirement for highly radiation-tolerant silicon microstrip sensors suitable for the SLHC application, we have fabricated n-in-p microstrip sensors in p-FZ and p-MCZ industrial wafers which we then irradiated with 70 MeV protons. Studies were made of the leakage current, onset of microdischarge, body capacitance, charge collection efficiency, and n-strip isolation at the fluences of nil, 0.7×10^{14}, and 7×10^{14} 1-MeV neutrons equivalent (neq)/cm^2. The bias and edge structure achieved holding the bias voltages up to 1000 V. The full depletion voltages were about 160, 250, and 600 V in the p-FZ and 1190, 500, and 840 V in the p-MCZ at nil, low, and high fluences, respectively. The radiation damage helped to reduce the density of electron accumulation layer. The strip isolation in the p-MCZ sensors was found to be much better than in the p-FZ sensors; even the no-isolation structure isolated the strips at nil fluence at bias voltage above 50 V. The lower density of electron accumulation layer in the p-MCZ could be attributed to an order less interface trap density in the $\langle 1\,0\,0 \rangle$ surface than that of $\langle 1\,1\,1 \rangle$, the negative potential in the inter-strip region by the bias voltage, and the possible effect of high oxygen content in the MCZ bulk.

PACS: 29.40.W; 81.40.W

Keywords: p-Bulk; Silicon; Microstrip; Sensor; Detector; Irradiation; Radiation damage

1. Introduction

The 14 TeV centre-of-mass proton–proton colliding accelerator at CERN, the large hadron collider (LHC) [1], is about to start collisions at the end of 2007. In order to exploit the physics potential of the LHC maximally, a major luminosity upgrade (SLHC) [2] is planned after the LHC has accumulated an integrated luminosity of 700 fb^{-1}. The instantaneous luminosity will be increased to 10^{35} from the 10^{34} cm^{-2} s^{-1} of LHC. Each experiment will accumulate an integrated luminosity of about 3000 fb^{-1}, thus reducing the statistical errors by half, and in addition enabling access to fundamental processes such as Higgs self-coupling [3].

In the inner detector of the ATLAS detector, the total fluence of the particles at a radius of 30 cm, normalized to an equivalent number of 1-MeV neutrons scaled with the non-ionizing-energy-loss (NIEL) values [4], will be $\sim 2 \times 10^{14}$ 1-MeV neq/cm^2 at the LHC (700 fb^{-1}) and $\sim 9 \times 10^{14}$ 1-MeV neq/cm^2 at the SLHC (3000 fb^{-1}) including similar safety factors of two. The radial region of 30–60 cm of the inner detector is currently equipped with the p-strips in n-bulk (p-in-n) silicon microstrip sensors, the SemiConductor Tracker (SCT) [5], which are designed only to cope with the fluence expected in the LHC. The p-in-n sensors, after type inversion of the bulk due to the radiation damage, require full depletion to collect charges efficiently [6]. With the increased fluence expected in the SLHC, the p-in-n sensor would no longer be fully depleted.

In order to cope with the very high fluence of the SLHC with a reasonably low bias voltage, new silicon microstrip sensors being designed are to be read out from the n-strips,

*Corresponding author. Tel.: +81 29 864 5791; fax: +81 29 864 2580.
E-mail address: yoshinobu.unno@kek.jp (Y. Unno).

0168-9002/$ - see front matter © 2007 Elsevier B.V. All rights reserved.
doi:10.1016/j.nima.2007.05.256

fabricated either in n-bulk or p-bulk material. Since acceptor states are created by radiation damage, the silicon bulk will inevitably become p-bulk and thus the n-strips become the side of p–n junction and full depletion will not be required. In the case the initial material is n-bulk, the sensor is denoted as n-strips in n-bulk (n-in-n); in the case of p-bulk, it is denoted as n-strips in p-bulk (n-in-p). The n-in-n sensor requires the p–n junction to be on the backside that entails double-sided mask processing. The n-in-p sensor requires single-sided mask processing which is more cost-effective, and thus a natural choice for large-area applications. Another possibility is the use of wafer material in which the full depletion voltage develops more slowly as a function of fluence, as shown by RD50 with the oxygen-rich materials grown with the Czochralski method [7]. Realization of the n-in-p silicon microstrip sensors for high fluence environments has several further technical design issues: (1) edge structure holding high bias voltage, (2) strip-region structure suppressing the onset of the microdischarge, and (3) isolation structure of the n-strips.

2. n-in-p R&D sensor fabrication

We have previously shown the potentiality of n-in-p microstrip sensors for the LHC application [8,9]. Those sensors were fabricated in p-bulk wafers made with the float-zoning method to a resistivity of about 10 kΩ cm. Working towards the SLHC application, a new program of R&D into n-in-p sensors has been initiated with the wafer materials available in industry in Japan [10]: p-type with the float-zoning method (p-FZ; resistivity of 5–10 kΩ cm, orientation of ⟨1 1 1⟩ or ⟨1 0 0⟩) and p-type with the magnetic-field applied Czochralski method (p-MCZ; 0.6–1 kΩ cm, ⟨1 0 0⟩). Other materials: n- or p-type with the standard Czochralski method (CZ) (~10 Ω cm) and n-type MCZ (n-MCZ) (~100 Ω cm) are not regarded as suitable due to the initial high full depletion voltages (FDVs).

A new batch of R&D sensors, called ATLAS05, was fabricated in 4-in. wafers: p-FZ of 8–20 kΩ cm and ⟨1 1 1⟩, and p-MCZ of 0.7–1 kΩ cm and ⟨1 0 0⟩. The n-strip isolation structures were implemented in six different zones as in the Ref. [10]. As the full depletion voltage of the p-bulk of 1 kΩ cm is expected to be about 950 V, we have set the maximum operation voltage of the sensor to be 800 V and the design bias voltage to be 1000 V. As the ATLAS05 sensors showed relatively low onset voltages of microdischarge, as described in the next section, the mask set was modified and another batch of R&D sensors, called ATLAS05-M, was fabricated out of the same lot of wafers as ATLAS05. The layout of ATLAS05-M mask set is shown in Fig. 1. The features of ATLAS05 and ATLAS05-M are summarized in Table 1. All the results given in this paper were made with 1 cm × 1 cm miniature sensors.

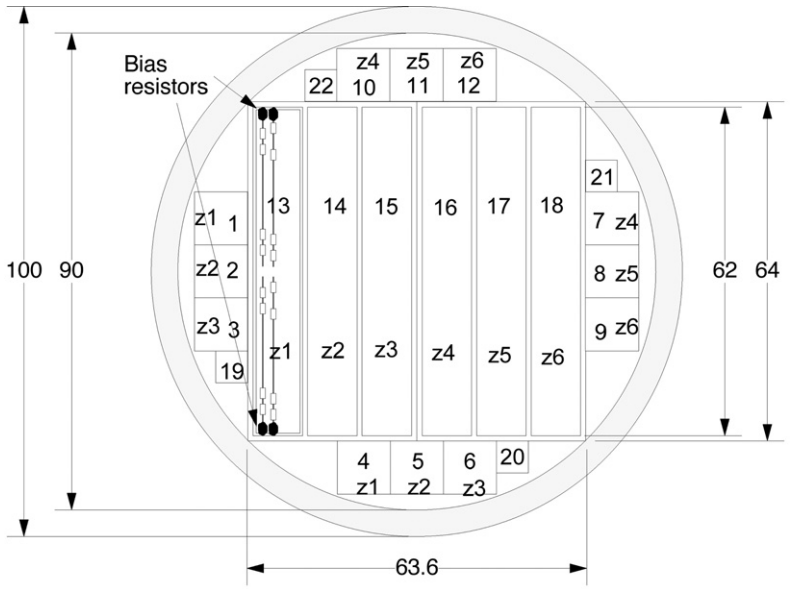

Features:
Main sensor with 6 zones:
2 longitudinal strips (3cm each) in a zone
80 um pitch strips in a zone
4 bonding pads per strip
1 bias ring for a zone
1 bias resistor per strip at end as shown
12 10mm x 10mm miniature sensors
4 monitor diodes

Zones:
z1: No p-stop
z2: Individual p-stop
z3: Common p-stop
z4: Individual p-stop with DC-field plate
z5: Common p-stop with DC-field plate
z6: No p-stop with AC-field plate

Fig. 1. Layout of the ATLAS05-M R&D sensors.

Table 1
Summary of ATLAS05 and ATLAS05-M R&D sensors

Features	ATLAS05/ ATLAS05-M
Thickness (μm)	300
Material	p-type FZ / p-type MCZ
Resistivity (kΩ cm)	8–20 / 0.7–1
Orientation	⟨1 1 1⟩ / ⟨1 0 0⟩
n-strip pitch (μm)	80
p-isolation type 1 (p-spray + p-stop) doping concentration[a] (ions/cm^2)	$1\times10^{12}+1\times10^{12}$/ $2\times10^{12}+2\times10^{12}$
p-isolation type 2 (p-stop) doping concentration[a] (ions/cm^2)	$1\times10^{12}/5\times10^{12}$
p-isolation type 3 (p-stop) doping concentration[a] (ions/cm^2)	2×10^{13}
Zone z1 (NPSTP)	No p-stop
Zone z2 (IPSTP)	Individual p-stop
Zone z3 (CPSTP)	Common p-stop
Zone z4 (IPSTPDF)	Individual p-stop with DC-field plate
Zone z5 (CPSTPDF)	Common p-stop with DC-field plate
Zone z6 (AF)	No p-stop with AC-field plate
DC pads	Aligned/staggered
No. of miniature sensors per zone per wafer	1/2

[a]The concentration values are approximate and indicative only.

3. Leakage current measurement and microdischarge—pre-irradiation

On receiving the fabricated sensors, the first concern was whether they could hold high bias voltage and exhibit low leakage current up to the design voltage of 1000 V. The bias voltage is to be held not only in the p–n junctions in the strip region but also in the edge structure between the bias ring that surrounds the strip region and the sensor edges. The edge structure is critical to achieve high voltage and low leakage current. The leakage currents of the ATLAS05 miniature sensors of the p-isolation type 3 as functions of bias voltages are shown in Fig. 2: the p-FZ (top figure) and the p-MCZ (bottom figure). Although most of the strip-isolation structures show onsets of microdischarge, one sensor, AF, shows smooth leakage current behavior up to 1000 V, both in the p-FZ and in the p-MCZ materials. As the edge structure of all sensors is the same, the edge-structure design has achieved the goals for high voltage and low leakage current. The other p-isolation types, however, showed much higher leakage currents from the low bias voltages, attributed to too low doping concentrations in the edge structure.

The next concern was the onset of the microdischarge. In the p-FZ sensors, the onsets were observed above 700 V and in the p-MCZ around 350 V. Visualization of the discharging location in the p-MCZ samples with the hot-electron analysis equipment revealed hot spots at the corner of the DC contact pads between the pads and the p-stop as shown in Fig. 3. As the narrow gap was thought

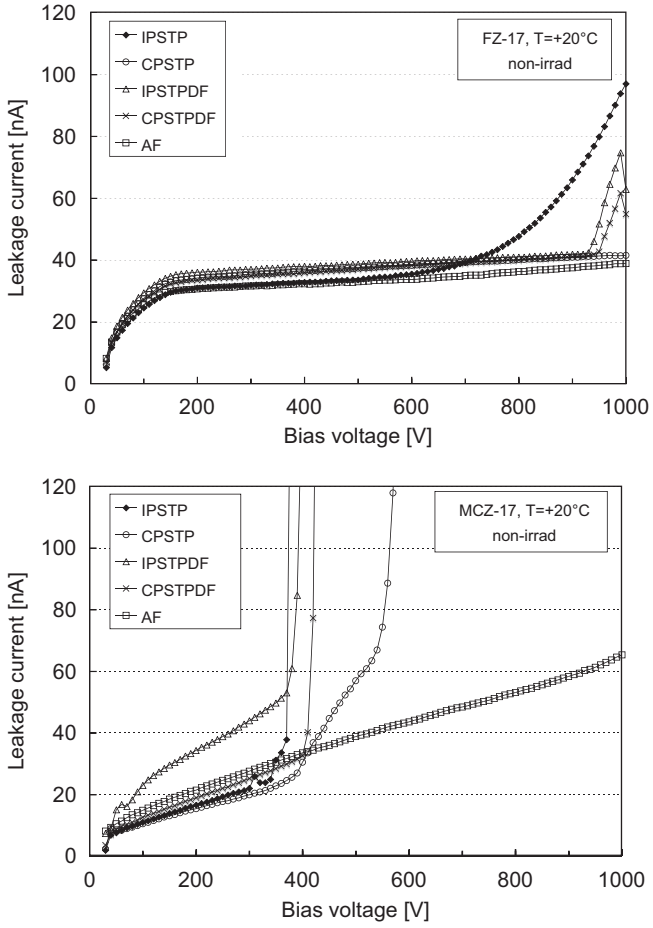

Fig. 2. Leakage current plots as functions of bias voltages of the miniature sensors of the p-isolation type 3 in the p-FZ (top) and the p-MCZ (bottom).

to have caused the onset of the microdischarge, a modified mask set, ATLAS05-M, was laid out to widen the gap by staggering the DC pads, together with other widening of the gaps between the n-strip and p-stop structures. The leakage current performance of the ATLAS05-M miniature sensors in the p-MCZ is shown in Fig. 4. The onset voltages of microdischarge of the p-stops without DC-field plate were improved to be above 500 V.

The onset voltages of the ATLAS05-M sensors with p-stops with DC-field plates were the same as those of the ATLAS05 sensors. A photo of the hot spots of the sensors identified with the hot-electron equipment is shown in Fig. 5. The photo shows not only the location of the high electric field around the end of the n-strips but also vital information that the luminous point was at the n-strip side contrary to the expectation at the p-stop side.

4. Irradiation

4.1. Irradiation facility and fluences

The ATLAS05 miniature sensors were irradiated with the protons at the Cyclotron and Radioisotope Center

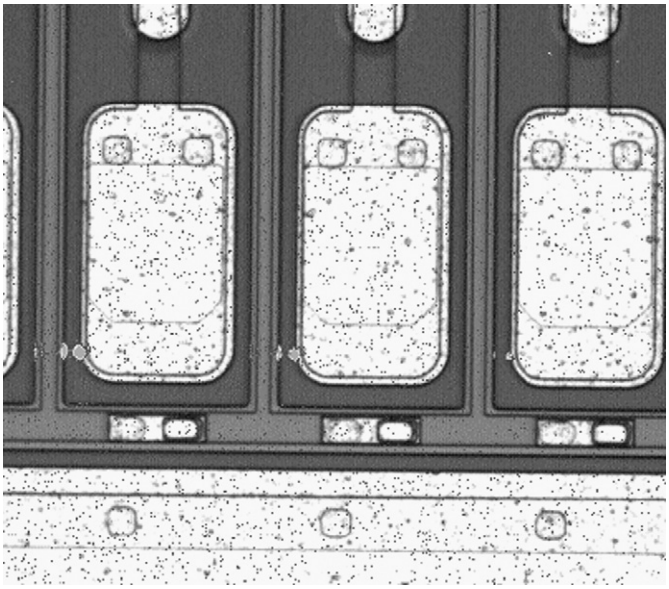

Fig. 3. Photograph of hot spots in the ATLAS05 R&D miniature sensor (CPSTPDF) made in the p-MCZ material. The spots are at a corner of the DC contact pads between the pads and the p-strip implantation.

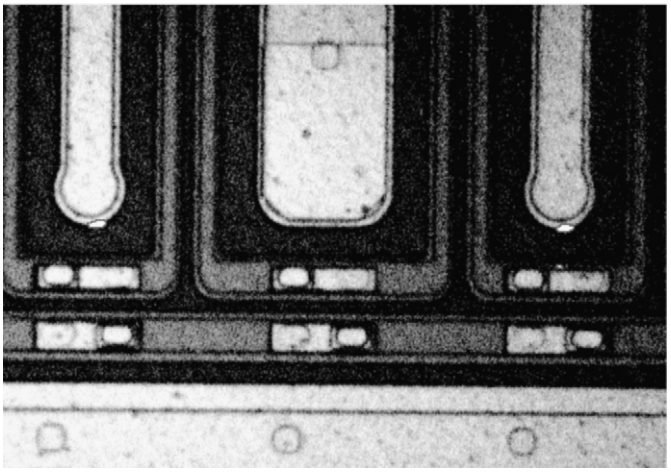

Fig. 5. Hot spots in the ATLAS05-M p-MCZ sensor with the p-stop structure with DC-field plate (IPSTPDF). Note that the larger luminous points are at the n-strip side.

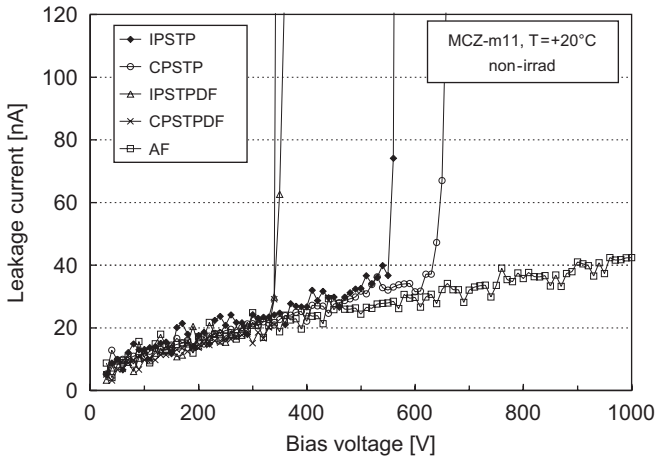

Fig. 4. Leakage current plots as a function of bias voltages of the miniature sensors in the p-MCZ of the modified mask set, ATLAS05-M. The onset voltages of microdischarge of the p-stops without DC-field plate were improved to be above 500 V.

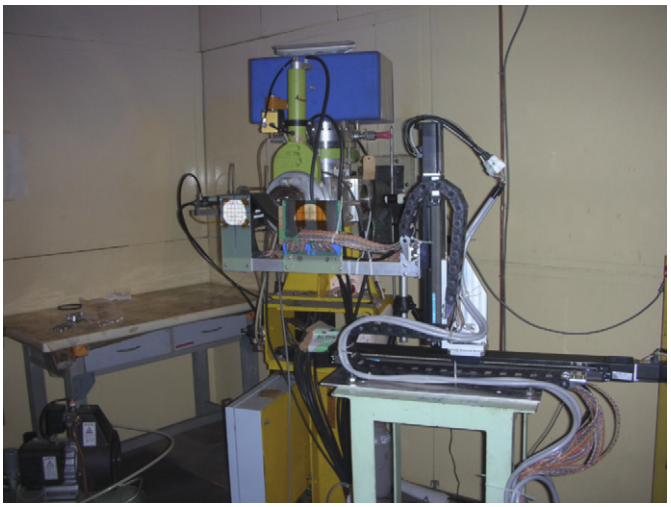

Fig. 6. The irradiation setup at the beamline 31-1 of the 930 AVF cyclotron. The irradiation box where a white circular fluorescence foil was attached was scanned with the X–Y stage whose black horizontal and vertical stages were seen in the right side.

(CYRIC) at Tohoku University [11]. The protons were accelerated to a kinetic energy of 70 MeV with the azimuthally varying field (AVF) cyclotron of a magnet radius of 930 mm with the accelerating radio frequency of 11–22 MHz and extracted to the beamline 31-2. The maximum beam current of the beamline was 500 nA and the full-width at half-maximum (FWHM) of the beam spot was about 5 mm.

Two sets of samples were prepared and irradiated [12]: one set at a low current of 10 nA reaching a fluence of 0.7×10^{14} 1-MeV neq/cm^2, the low-fluence samples; and the other at a high current of 100 nA reaching 7×10^{14} 1-MeV neq/cm^2, the high-fluence samples. The proton fluences were evaluated with aluminum foil activation dosimetry. The error in dosimetry was estimated to be about 10% at most. A photo of the setup of the irradiation is shown in Fig. 6. Since the miniature sensors had an area of 1 cm × 1 cm, the samples were scanned in the beam over an area of 2 cm × 2 cm in an X–Y scanning stage of 50 cm (horizontal: X) and 20 cm (vertical: Y) long. The 1-MeV neutron equivalent fluences were deduced from the 70 MeV proton fluences by using the NIEL damage ratio of 0.7 protons at 70 MeV to neutrons at 1 MeV.

During the irradiation, the samples were biased at 20–60 V depending on the maximum leakage current. No cooling was applied. After the irradiation, they were kept in a freezer at −20 °C unless otherwise mentioned. Before post-irradiation measurements, they were annealed for 4

days at a temperature of +25 °C. The measurements in the next sections were carried out at −20 °C.

4.2. Leakage current measurement (IV)

The leakage current as a function of bias voltage of the samples of the fluence of 0.7×10^{14} 1-MeV neq/cm^2 are shown in Fig. 7 and of the 7×10^{14} in Fig. 8: the p-FZ (top) and the p-MCZ (bottom). In both cases, the bias voltage could be held up to 1000 V. In the low fluence samples, the onsets of microdischarge of the p-FZ were seen around 400 V for all isolation structures including the AF structure. Also, the leakage currents in the isolation structures were scattered widely in both the p-FZ and p-MCZ samples. In the high fluence, the leakage currents behaved well. Onsets of microdischarge were not observed except in one structure for which the onset voltage was relatively high, 700 V.

The onsets of microdischarge of the low fluence p-FZ samples, especially of the AF structure, may imply that the location of the source is not in the isolation structure but in a structure that is common to all samples. This low fluence behaviour, as well as the scattering of leakage currents, needs close attention in future studies.

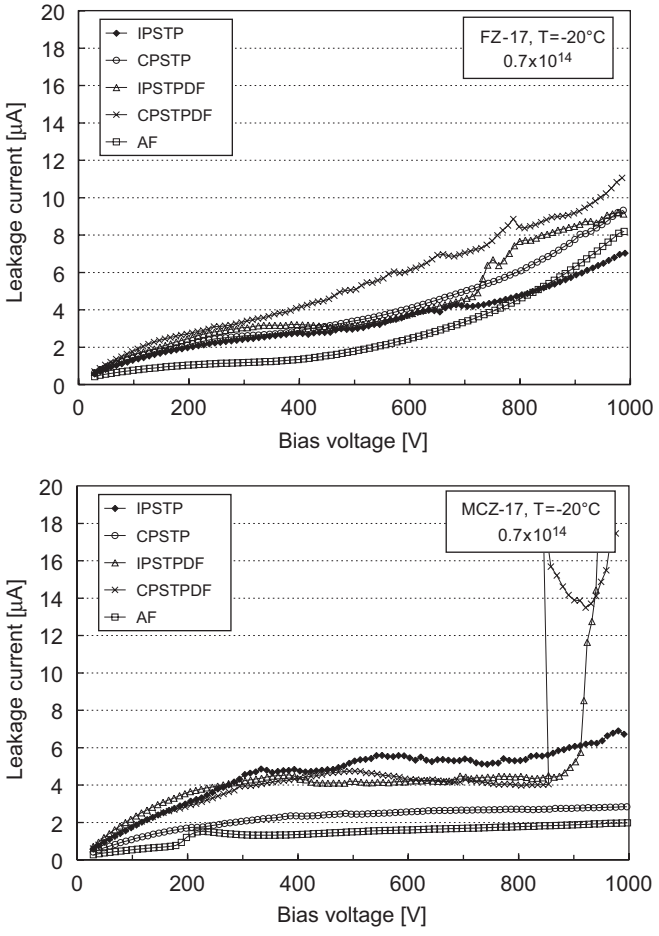

Fig. 7. Leakage current plots as functions of bias voltages measured at a temperature of −20 °C for the fluence of 0.7×10^{14} 1-MeV neq/cm^2: p-FZ sensors (top) and p-MCZ sensors (bottom).

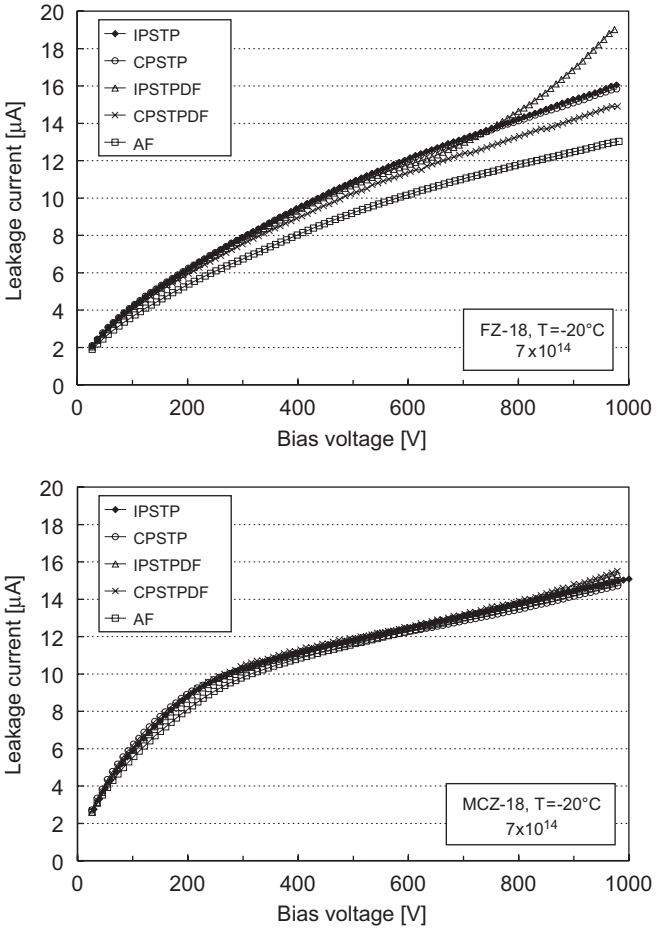

Fig. 8. Leakage current plots as functions of bias voltages measured at the temperature of −20 °C for the fluence of 7×10^{14} 1-MeV neq/cm^2: p-FZ sensors (top) and p-MCZ sensors (bottom).

4.3. Body capacitance measurement (CV)

The body capacitance was measured between the bias ring and the backplane as a function of bias voltage at a frequency of 1 kHz. The strips in the strip region are connected to the bias ring through bias resistors of 1.5 MΩ each. The capacitance between the bias ring and the backplane is thus the capacitance between the strips and the backplane at frequencies where impedance contributions of the bias resistors are negligible. The plots of the inverse of the body capacitance squared, $1/C^2$, are shown in Fig. 9. Since the thickness of the depleted region expands as the square root of the bias voltage, the body capacitance decreases as the inverse square root of the voltage. Thus, the inverse of the capacitance squared increases linearly as a function of the bias voltage, and levels off at a value defined by the geometrical thickness once the bulk is fully depleted. The capacitances were averaged over the samples of various isolation structures in the same batch of material, as the body capacitance was independent of the

isolation structure for a given fluence. The linear behavior of the capacitance was clearly seen as expected except in the p-FZ samples. The p-FZ non-irradiated batch had a second slope at medium voltage range and its bias voltage was limited to 750 V due to microdischarge in the batch. The cause of the second slope is yet to be understood. The intersecting points of the linear increases and the plateau values were regarded as the FDV of the batches. The FDVs are summarized in the columns labeled evaluation method "FDV (CV)" in Table 2 and shown in Fig. 11.

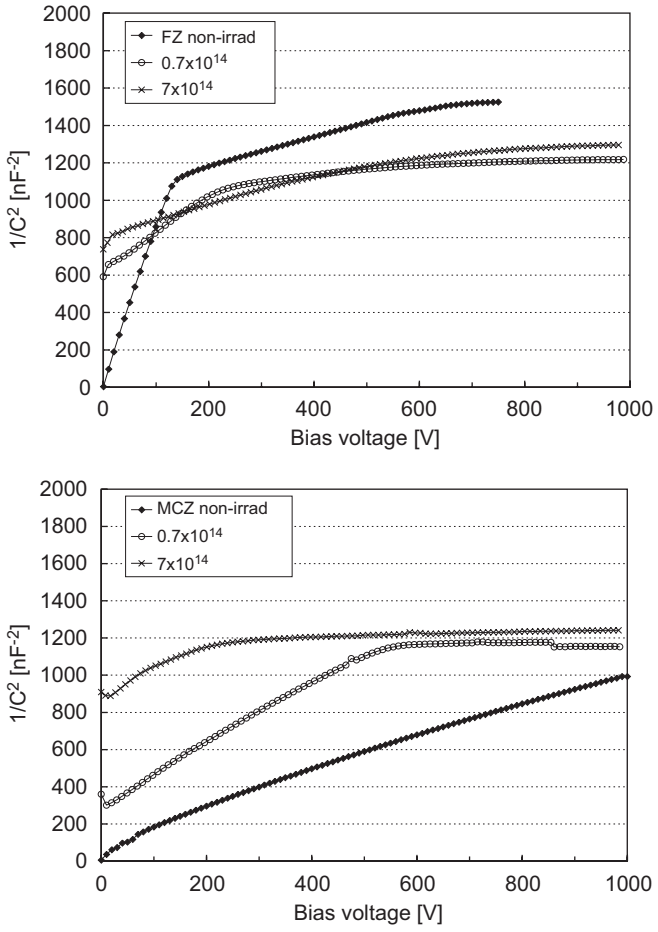

Fig. 9. Body capacitance plots, $1/C^2$, as functions of bias voltages: the p-FZ (top) and p-MCZ (bottom) samples for the fluences of nil (filled diamond), 0.7×10^{14} 1-MeV neq/cm^2 (open circle), and 7×10^{14} (cross).

4.4. Charge collection efficiency (CCE) measurement

The CCEs as a function of bias voltage were measured by generating electron–hole pairs in the depleted region with a 1064-nm laser [9,13]. A single amplifier channel was used for each measurement, connected in turn, with the signals amplified and then averaged by a digital oscilloscope. The amplifier was a base-grounded current amplifier and had a gain of 3 mV/fC, a polarity suitable for the signals, and a shaping time constant of about 20 ns. The low gain was compensated by a large signal from the laser. The laser power was monitored with a reference sample set adjacent to the device-under-test in a cooling box. The box was flushed with cold nitrogen gas in order to avoid icing on the surface of the samples. The laser was focused to a spot size of 3 μm on the surface with a convergence angle of about 100 mrad. The laser exited the backside with an estimated radius of about 10 μm after refraction.

The CCEs of the AF samples were measured with the gate voltage at 60 V (see the next section). The results are shown in Fig. 10: the p-FZ sensors (top) and the p-MCZ (bottom); and the fluences of nil (filled diamond), 0.7×10^{14} 1-MeV neq/cm^2 (open circle), and 7×10^{14} (cross). The CCEs were normalized to the saturated value of the p-FZ nil fluence sample. As with the body capacitance, the collected charges are expected to be linear with the depletion depth and proportional to the square root of bias voltages. By plotting the square of the CCE, CCE^2, as a function of bias voltage, the FDV were estimated from the intersection of the linear increases and the saturated levels. These FDV results are summarized in Table 2, in the columns labeled "FDV (CCE)", and plotted in Fig. 11. The saturated values of the CCEs are also summarized in Table 2. Although some charge loss is apparent, it is still small with the CCEs about 80% at high fluence.

The FDVs obtained by the two methods, CV and CCE, were consistent with each other except for the p-MCZ at high fluence. In the p-MCZ samples, the CV, and in addition the IV behaviour (Fig. 8, bottom), implied the low FDV clearly. The high FDV with the CCE method may imply large charge capture and emission with the bias voltage in the highly radiation damaged p-MCZ material. This is yet to be understood.

Table 2
Summary of the estimated full depletion voltages of the p-FZ and the p-MCZ wafers of 300 μm

Evaluation method	Material					
	p-FZ			*p*-MCZ		
	FDV (CV)	FDV (CCE)	CCE	FDV (CV)	FDV (CCE)	CCE
Non-irradiation	175	150	1	1190	1180	1
0.7×10^{14} 1-MeV neq/cm^2	285	210	0.9	525	485	0.8
7×10^{14} 1-MeV neq/cm^2	635	565	0.8	260	845	0.8

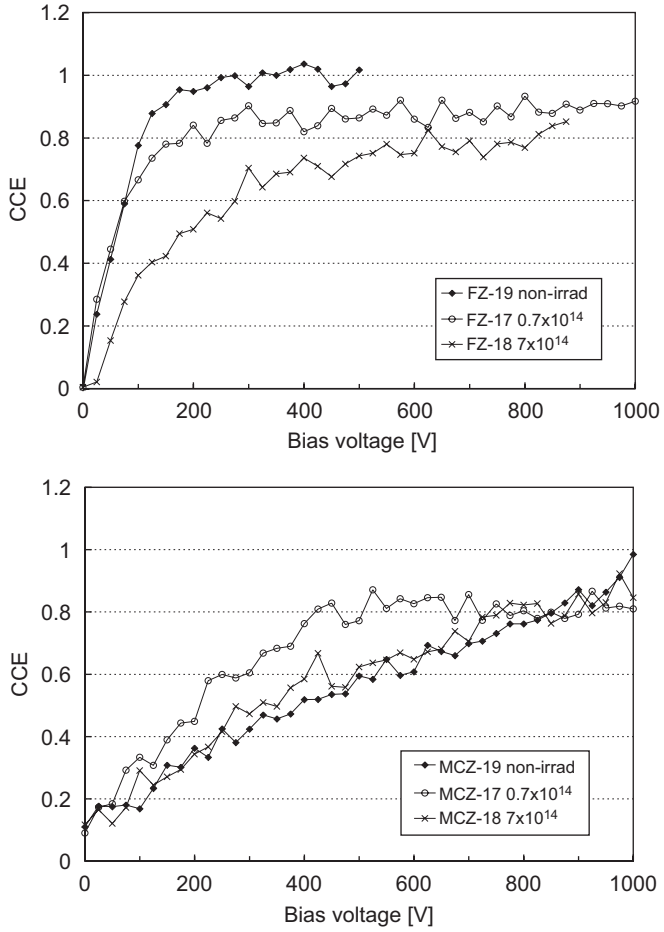

Fig. 10. Charge collection efficiencies as functions of bias voltages measured with a 1064-nm laser: p-FZ (top) and the p-MCZ (bottom) sensors for the fluences of nil (filled diamond), 0.7×10^{14} 1-MeV neq/cm^2 (open circle), and 7×10^{14} (cross).

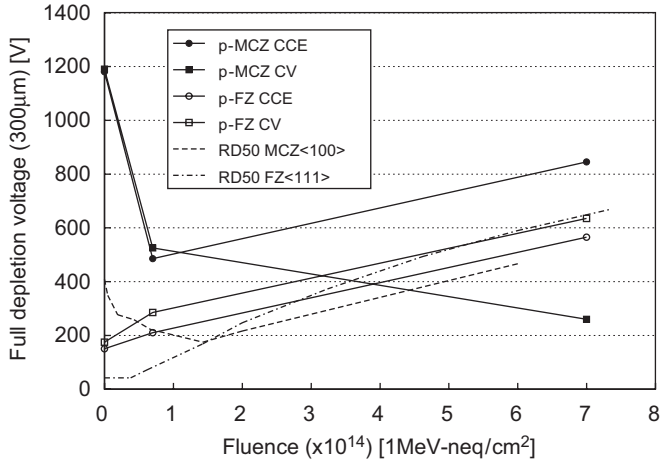

Fig. 11. Full depletion voltages of 300-μm thick wafers as a function of fluence, estimated with the capacitance (CV, squares) and the charge collection efficiency (CCE, circles) methods for the p-FZ (open square/circle), and the p-MCZ (filled square/circle) samples. The plots of the n-FZ (dot–dash) and n-MCZ (dash) are overlaid from Ref. [7].

4.5. Strip isolation measurement

Due to positive oxide charges and the trap charges in the interface between the silicon bulk and the SiO_2 layer at the surface, electrons attracted to the positive charges develop an electron accumulation layer that shorts the n-strips. The n-strip isolation structures with p-implantation are to interrupt this accumulation layer. The isolation of the n-strips was characterized by measuring the current between a pair of n-strips, the "inter-strip current", when a voltage of 5 V was applied between the pair. When the isolation resistance is larger than the sum of the bias resistors of the pair, i.e., 3 MΩ, the inter-strip current levels off at 1.6 μA. The maximum current was limited with an external resistor of 5 kΩ. The inter-strip currents as functions of bias voltage are shown in Fig. 12: the p-FZ (top) and the p-MCZ sensors (bottom) for the isolation structure and the fluence combinations.

In the p-FZ case, the NPSTP sample, i.e., with no isolation structure, had no isolation up to the bias voltage

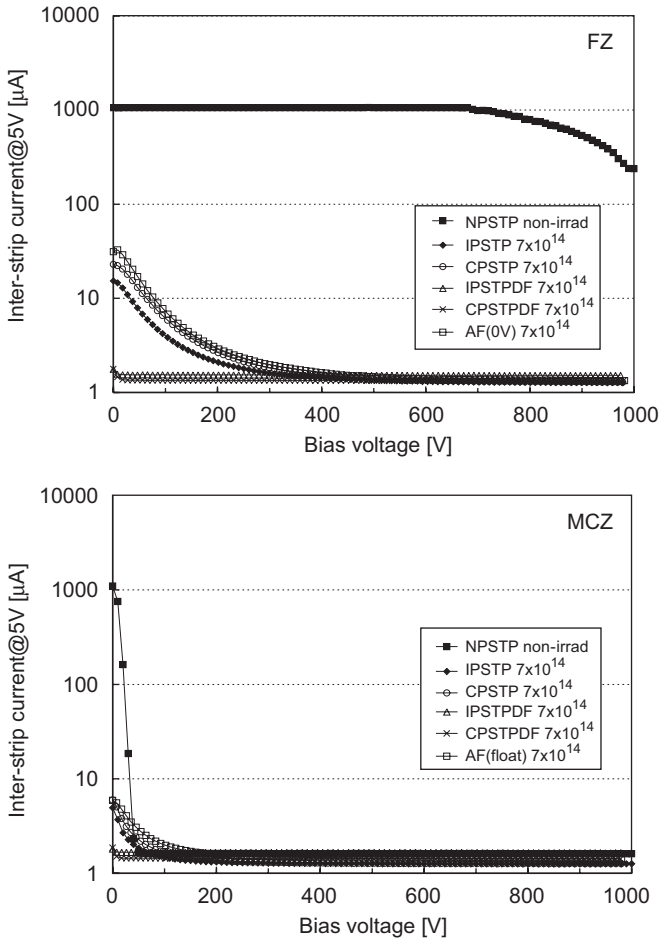

Fig. 12. The inter-strip currents between pairs of the n-strips by applying 5 V between the pairs as functions of bias voltages: p-FZ (top) and p-MCZ (bottom); the isolation structure of NPSTP of the nil fluence (filled square) and IPSTP (filled diamond), CPSTP (open circle), IPSTPDF (open triangle), CPSTPDF (cross), and AF (gate voltage of 0 V, open square) of 7×10^{14} 1-MeV neq/cm^2.

of 1000 V, as expected. All other p-implantation isolation structures achieved isolation in the nil, low and high fluences. In the high fluence case, however, the no-isolation structure manifested by the AF (gate voltage of 0 V) achieved isolation at the bias voltage above 500 V. This was contrary to the expectation that the radiation damage created more oxide charges, which would eventually saturate, with no isolation achieved. The radiation damage in the silicon bulk and in the oxide layer may have hardened the interface and compensated the interface charges with the help of the bias voltage. Also, in the high-fluence case, the IPSTP and the CPSTP isolation structures behaved much like the AF (gate voltage of 0 V).

In the p-MCZ sensors, the isolation was much better than in the p-FZ. Even at nil fluence, the no-isolation structure sample, NPSTP, achieved isolation with bias voltage above 50 V. The high fluence deterioration of the isolation was also much less than for the p-FZ. The isolation at low fluence was as good as or better than at high fluence.

The density of the electron accumulation layer can be quantified by applying a voltage to the AF field plate, the gate voltage, compensating the positive interface charges. The inter-strip currents of the AF samples in the p-FZ as a function of the gate voltage are shown in Fig. 13. A bias voltage of 200 V was applied to the silicon bulk during the measurement. At nil fluence, a large gate voltage of more than 40 V was required for the compensation, while at low and high fluences, the required gate voltage was as small as 10 V, thus confirming the lower density of the accumulation layer in the radiation damaged interfaces. In the p-MCZ samples, no gate voltage was required for the compensation as the bias voltage of 200 V was applied. The polarity of the gate and the bias voltages were negative with respect to the potential of the n-strips.

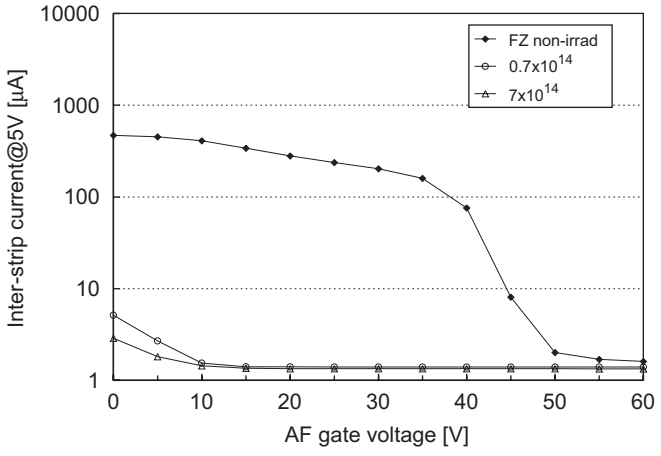

Fig. 13. The inter-strip currents between pairs of the n-strips of the p-FZ sensors as a function of gate voltage to the AF field plate: the fluences of nil (filled diamond), 0.7×10^{14} (open circle), and 7×10^{14} 1-MeV neq/cm^2 (open triangle). The bias voltage of 200 V was applied to the bulk.

4.6. Discussion

We found that p-MCZ did not require a structure to isolate the n-strips. This indicated low density of the electron accumulation layer in the interface. This is in accordance with the observation that the hot spots were in the n-strip side in the p-MCZ sensors. If there were a conductive electron accumulation layer, the high electric field would appear in the junction of the accumulation layer and the p-implantation, i.e., at the edge of the p-stop structure.

The low density of the electron accumulation layer can be attributed to (1) a significantly lower interface trap density in the $\langle 1\,0\,0 \rangle$ than the $\langle 1\,1\,1 \rangle$ surface [14], (2) the possibility that the high oxygen concentration of order 10^{18} ions/cm^3 in the p-MCZ material might have helped to reduce the interface charges, and (3) an order higher acceptor concentration in the p-MCZ than in the p-FZ material. The bias voltage that provides negative potential in the inter-strip regions helps nullify the electron accumulation layer.

5. Summary

Working towards highly radiation-tolerant silicon microstrip sensors suitable for the SLHC application, we have fabricated n-in-p microstrip sensors in p-FZ and p-MCZ industrial wafers, with various n-strip isolation structures, which were irradiated with 70 MeV protons at the CYRIC at Tohoku University. Studies were made of leakage current, onset of microdischarge, body capacitance (CV), charge collection efficiency (CCE), and n-strip isolation, at nil, 0.7×10^{14} and 7×10^{14} 1-MeV neq/cm^2 fluences.

The bias and edge structure has achieved holding bias voltage up to 1000 V with low leakage current. Onset of microdischarge was observed at the edge of n-strips. Although improvements have been made, further improvement is necessary to drive the onset near to or above 800 V. The full depletion voltages (FDV) were evaluated with the CV and CCE measurements. The FDVs were about 160, 250, and 600 V in the p-FZ and 1190, 500, and 840 V in the p-MCZ samples, at the nil, low, and high fluences, respectively. The CCE at high fluence was about 80%. The inconsistency in the FDV observed in the CV and CCE needs attention in future studies.

All the p-implanted isolation structures isolated the n-strips. The no-isolation structure did not isolate the strips in the p-FZ sample at the nil fluence. It did prove to be isolated, however, at low and high fluences once the bias voltage was above 500 V. The isolation in the p-MCZ samples was found to be much better than in the p-FZ samples. Even the no-isolation structure isolated the strips at the nil fluence at bias voltage above 50 V. The lower density of the electron accumulation layer in the p-MCZ could be attributed to a significantly lower interface trap density in the $\langle 1\,0\,0 \rangle$ surface, high oxygen content in the MCZ bulk, and high acceptor concentration in

low-resistivity material. The negative potential in the inter-strip region by the bias voltage helps nullify the electron accumulation layer.

References

[1] The LHC Conceptual Design Report—The Yellow Book, CERN/AC/95-05(LHC), 1995.
[2] The European Strategy for Particle Physics, approved by the CERN council, 14 July 2006 〈http://council-strategygroup.web.cern.ch/council-strategygroup/Strategy_Statement.pdf〉.
[3] F. Gianotti, et al., Physics Potential and Experimental Challenges of the LHC Luminosity Upgrade, CERN-TH/2002-078.
[4] A. Vasilescu (INPE Bucharest), G. Lindstroem (University of Hamburg), Displacement Damage in Silicon, On-Line Compilation, 〈http://sesam.desy.de/members/gunnar/Si-dfuncs.html〉.
[5] Y. Unno, Nucl. Instr. and Meth. A 511 (2003) 58; L. Feld, Nucl. Instr. and Meth. A 511 (2003) 183.
[6] Y. Unno, et al., IEEE Trans. Nucl. Sci. NS-49 (2002) 1868.
[7] M. Moll, et al., Nucl. Instr. and Meth. A 546 (2005) 99.
[8] S. Terada, et al., Nucl. Instr. and Meth. A 383 (1996) 159.
[9] K. Hara, et al., Nucl. Instr. and Meth. A 565 (2006) 538.
[10] Y. Unno, Nucl. Instr. and Meth. A 569 (2006) 41.
[11] Cyclotron and Radioisotopes Center (CYRIC), Tohoku University, 6-3 Aoba, Aramaki, Aoba-ku, Sendai, Miyagi 980–8578, Japan 〈http://www.cyric.tohoku.ac.jp/index-e.html〉.
[12] CYRIC 930 Experiment Number 8437, Contact persons: T. Shinozuka (CYRIC) and Y. Unno (KEK).
[13] Y. Unno, et al., Nucl. Instr. and Meth. A 383 (1996) 238.
[14] S.M. Sze, Physics of Semiconductor Devices, second ed., Wiley, New York, p. 386.